Investigation of birefringence in hematite under uniaxial mechanical stress in a magnetic field

V. S. Merkulov, E. G. Rudashevskiĭ, H. LeGall,[1)] and C. Leicuras[1)]

P. N. Lebedev Physics Institute, USSR Academy of Sciences
(Submitted 17 February 1978)
Zh. Eksp. Teor. Fiz. **75**, 628–640 (August 1978)

We have separated experimentally the magnetic, magnetostriction, and photelastic contributions to the birefringence in hematite (α-Fe_2O_3, T = 300K) in which radiation propagates along the C_3 axis and to which a mechanical stress is applied in a magnetic field. It is shown that the main contribution to the birefringence is of pure magnetic origin. The proposed optical method is used to investigate the magnetic orientational transition that occurs when mechanical stresses are applied in a magnetic field at 300 K. The existence of antiferromagetic domains in the region of the orientational transition was observed. Methods of making the sample single-domain are proposed.

PACS numbers: 78.20.Fm, 75.80. + q, 75.60.Ch

1. INTRODUCTION

In the study of birefringence in magnetically ordered crystals always includes the question of the nature of this phenomenon. The birefringence due to establishment of mangetic order can be caused either by the magnetic subsystem of the crystal or by the lattice deformation due to magnetostriction; the magnetostriction can make in turn a large contribution. It is therefore important to compare and separate these contributions if possible. In addition, it is of interest to investigate the possibilities of using magneto-optical methods for the study of orientational magnetic phase transitions.

For an experimental study of these questions we chose single-crystal hematite (α–Fe_2O_3). In the paramagnetic state it is a uniaxial crystal (space group D_{3d}^6) with a difference $n_0 - n_e = 0.2$ between the principal refractive indices,[1] where $n_0 = 2.84$ at the wavelength[2)] $\lambda = 1.15$ μm. Between the Néel temperature $T_N = 950$ K and the Morin temperature $T_M = 260$ K hematite has weak-ferromagnetic ordering that causes the crystal to become biaxial in a single-domain state, and the difference between the principal refractive indices in the basal plane reaches a value 0.2×10^{-3} at $T = 300$ K.[2]

Magnetic ordering leads also to magnetostriction that reaches values 7×10^{-6} in the basal plane[3] and contributes in turn to the birefringence. In the present study we subjected the hematite single crystal to a mechanical stress in order to cancel out the magnetostriction contribution to the birefringence and to compare it with the total value of the birefringence.[3)] In addition, we investigated by a magneto-optical method the previously observed[4,5] orientational magnetic phase transition induced by mechanical stress in an external magnetic field at $T = 300$ K.

2. EFFECT OF MAGNETIC SUBSYSTEM AND OF MECHANICAL STRESS ON BIREFRINGENCE IN HEMATITE

The linear birefringence in hematite at optical frequencies is determined by the dielectric tensor ε_{ij}, which is connected with the sublattice magnetizations M_1 and M_2 and with the strain tensor u_{ij} by the relation

$$\epsilon_{ij} = \epsilon_{ij}^0 + \xi_{ijkl} u_{kl} + \eta_{ijkl} l_k l_l + \alpha_{ijkl} l_k m_l + \beta_{ijkl} m_k m_l, \quad (1)$$

where ε_{ij}^0 is the tensor component that does not depend on the magnetic moments or the strains, $\mathbf{l} = (\mathbf{M}_1 - \mathbf{M}_2)/2M_0$, $\mathbf{m} = (\mathbf{M}_1 + \mathbf{M}_2)/2M_0$, $2M_0 = |\mathbf{M}_1| + |\mathbf{M}_2|$; ξ_{ijkl}, η_{ijkl}, α_{ijkl}, β_{ijkl} are the corresponding tensors (the subscripts $i, j, \ldots$ run through the values x, y, and z, and summation over the dummy indices is implied throughout). Since the birefringence in hematite remains constant at least up to [2] 20 kOe, we can neglect the terms with $l_k n_l$ and $m_k m_l$ in (1).

In view of the symmetry of the tensors $\varepsilon_{ij}, u_{ij}, l_i l_j$ it is convenient to use abbreviated subscripts $p, q, \ldots$ that run through the values $1, \ldots 6$, the relations between the subscripts ij and p being:

ij:	xx	xy	zz	yz	xz	xy
p:	1	2	3	4	5	6

Formula (1) then takes the form

$$\varepsilon_p = \varepsilon_p^0 + \xi_{pq} u_q + \eta_{pq} (ll)_q.$$

The components of the strain tensor u_p depend in turn on the external mechanical stresses σ_q and on the magnetic subsystem in the following manner:

$$u_p = s_{pq} \sigma_q + U_{pq} (ll)_q. \quad (2)$$

where s_{pq} is the compliance tensor and U_{pq} are the magnetostriction constants. After substituting the equilibrium strains (2), the dielectric tensor (1) takes the form

$$\varepsilon_p = \varepsilon_p^0 + (\eta_{pq} + \eta_{pq}') (ll)_q + \xi_{pq} \sigma_q, \quad (3)$$

where $\eta_{pq}' = \xi_{pr} U_{rq}$, $\xi_{pq} = \xi_{pr} s_{rq}$. We note that the selection rules for the tensors ξ_{pq}, η_{pq}, U_{pq}, ξ_{pq} are the same, since the components of the tensors ε_p, U_p, σ_p, $(ll)_p$ transform in accordance with the same representation of the factor-group $\tilde{D}_{3d}^6$. The selection rules for the components of the tensor U_{pq} (the z and x axes are parallel to C_3 and U_2, respectively) are

$$\begin{Vmatrix} U_{11} & U_{12} & U_{13} & U_{14} & 0 & 0 \\ U_{12} & U_{11} & U_{13} & -U_{14} & 0 & 0 \\ U_{31} & U_{31} & U_{33} & 0 & 0 & 0 \\ U_{41} & -U_{41} & 0 & U_{44} & 0 & 0 \\ 0 & 0 & 0 & 0 & U_{44} & 2U_{41} \\ 0 & 0 & 0 & 0 & U_{14} & U_{11} - U_{12} \end{Vmatrix}. \quad (4)$$

 0038-5646/78/080316-07$02.40

The components U_{pq} for hematite can be found in Refs. 3 and 7. The cancellation of the magnetostriction contribution $\eta'_{pq}(ll)_q$ with the aid of external mechanical stresses is in general a rather complicated task. However, in the particular case when l lies in the basal plane, the magnetostriction contribution can be cancelled by a uniaxial mechanical stress. Let all the components $\sigma_p = 0$ with the exception of $\sigma_2 = p$, and let $\mathbf{l} = (-\sin\varphi, \cos\varphi.0)$, as shown in Fig. 1. If the radiation propagates along the z axis, it suffices to consider the components of the dielectric tensor in the xy plane:

$$\varepsilon_{xx} = \varepsilon + (\eta + \eta')\cos 2\varphi + \zeta p,$$
$$\varepsilon_{yy} = \varepsilon - (\eta + \eta')\cos 2\varphi - \zeta p, \quad \varepsilon_{xy} = (\eta + \eta')\sin 2\varphi, \tag{5}$$

where

$$\varepsilon = \varepsilon_{xx}^0 + {}^1/_2(U_{11}+U_{12})(\xi_{11}+\xi_{12}) + \xi_{13}U_{31} + {}^1/_2(\eta_{11}+\eta_{12}) + {}^1/_2(\zeta_{11}+\zeta_{12})p,$$
$$\eta = -{}^1/_2(\eta_{11}-\eta_{12}), \quad \zeta = -{}^1/_2(\xi_{11}-\xi_{12}),$$
$$\eta' = -{}^1/_2(U_{11}-U_{12})(\xi_{11}-\xi_{12}) - U_{41}\xi_{14}.$$

If a sufficiently strong magnetic field is applied along the x axis, the vector l aligns itself with the y axis and $\varphi = 0$. From this we find that to cancel the magnetostriction contribution η' to the birefringence we must apply a pressure

$$p_s = -\frac{\eta'}{\zeta} = -\frac{{}^1/_2(U_{11}-U_{12})(\xi_{11}-\xi_{12}) + U_{41}\xi_{14}}{{}^1/_2(s_{11}-s_{12})(\xi_{11}-\xi_{12}) + s_{14}\xi_{14}} \tag{6}$$

Despite the fact that the photoelastic constants ξ_{pq} of hematite are unknown, this pressure can be estimated by assuming that $\xi_{14}/(\xi_{11} - \xi_{12}) \ll 1$. Favoring this assumption is the fact that in corundum (α–Al_2O_3), which has the same structure as hematite (α–Fe_2O_3), we have $\xi_{14}/(\xi_{11} - \xi_{12}) < 0.1$ (Ref. 8). Under this assumption, the counterbalancing uniaxial mechanical stress in hematite is equal to

$$p_s = \frac{U_{11}-U_{12}}{s_{11}-s_{12}} = 13\ \text{kgf/cm}^2.$$

3. BEHAVIOR OF MAGNETIC SUBSYSTEM UPON APPLICATION OF A UNIAXIAL MECHANICAL STRESS

In the general case, the thermodynamic potential of a magnetically ordered cyrstal in a magnetic field, to which mechanical stresses are applied, consists of three parts:

$$\Phi = \Phi_m + \Phi_{me} + \Phi_{el}, \tag{7}$$

where $\Phi_{el} = 1/2 c_{ijkl}u_{ij}u_{kl} - \sigma_{ij}u_{ij}$ is the energy of the elastic deformations, c_{ijkl} is the elastic-moduli tensor; $\Phi_{me} = \delta_{ijkl}u_{ij}l_k l_l$ is the magnetoelastic part and Φ_m is the magnetic part. Minimization of such a potential yielded formula (2) for the equilibrium strains, with $U_{ijkl} = -s_{ijmn}\delta_{mnkl}$. After substituting the equilibrium strains

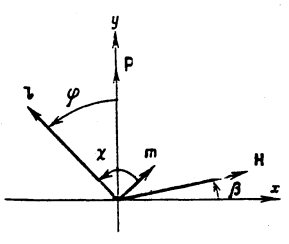

FIG. 1. Orientations of the vectors **H**, **p**, **l**, and **m** relative to the laboratory xy frame.

(2) in (7) we obtain for the thermoydnamic potential

$$\Phi = \Phi_m' - U_{ijkl}\sigma_{ij}l_k l_l - {}^1/_2 s_{ijkl}\sigma_{ij}\sigma_{kl}. \tag{8}$$

The prime of Φ_m' denotes that it includes invariants of fourth order in l_i of magnetostriction origin, but when the static properties are considered these do not differ at all from the pure magnetic invariants.

We have thus obtained a potential from which the variable u_{ij} has been eliminated. This is convenient for finding the equilibrium orientation of the spin system.

Consider the behavior of the spin system in the particular case when l, m, and H lie in the basal plane and a uniaxial mechanical stress is applied to the hematite crystal (Fig. 1). The thermodynamic potential takes then the form

$$\Phi = {}^1/_2 Bm^2 + q(l_x m_y - l_y m_x) + {}^1/_2 D(\mathbf{ml})^2 - 2M_0\mathbf{mH} - {}^1/_2(U_{12}-U_{11})(l_x^2 - l_y^2)p. \tag{9}$$

The expression for Φ_m is taken here from Ref. 9 under the assumption that the anisotropy in the basal plane is small.

Introducing the variables in accord with Fig. 1 and minimizing the potential (9) with respect to the variables φ, χ, and m, we obtain the equilibrium orientation of the vector l as determined by the angle φ, using the equation

$$(U_{12}-U_{11})p\sin 2\varphi = m_D H\sin(\varphi-\beta) + (\chi_\perp - \chi_\parallel)H^2\sin 2(\varphi-\beta), \tag{10}$$

where

$$m_D = 2M_0 q/B, \quad \chi_\perp = (2M_0)^2/B, \quad \chi_\parallel = (2M_0)^2/(B+D).$$

In the important particular case when $\mathbf{H} \perp \mathbf{p}$, i.e., $\beta = 0$, the rotation of the vector l as a function of the magnetic field at $p = \text{const} > 0$ has the character of a second-order phase transition, namely,

$$\varphi = 0 \quad \text{at} \quad H \geqslant H_{cr}, \tag{11}$$

$$\varphi = \arccos\frac{m_D H}{2[(U_{12}-U_{11})p - (\chi_\perp - \chi_\parallel)H^2]}, \quad \text{at} \quad 0 \leqslant H \leqslant H_{cr}, \tag{12}$$

where

$$H_{cr} = \frac{[m_D^2 + 16(U_{12}-U_{11})(\chi_\perp - \chi_\parallel)p]^{1/2} - m_D}{4(\chi_\perp - \chi_\parallel)}. \tag{13}$$

If $\chi_\parallel = 0$, formulas (12) and (13) agree with those given in Ref. 10. At $p \ll m_D^2/16(U_{12} - U_{11})(\chi_\perp - \chi_\parallel) \sim 10^3$ kgf/cm^2, corresponding the experimental conditions, formulas (12) and (13) become much simpler and take the form

$$H_{cr} = \frac{2p(U_{12}-U_{11})}{m_D}, \quad \varphi = \arccos\frac{H}{H_{cr}} \quad \text{at} \quad 0 < H < H_{cr}.$$

It is important that in this orientation the rotation of l is even in φ, i.e., formation of an antiferromagnetic domain structure is possible. This degeneracy is lifted by $\beta \neq 0$ when a constant component of the magnetic field H_y is applied. Allowance for sixth-order anisotropy in the basal plane also lifts the degeneracy of the twofold axis U_2 is not parallel to H.

When $0 < \beta < \pi/2$ and $p > 0$, the minimum of the potential (9) corresponds to solution of an equation with $\varphi \to \beta$ as $H \to \infty$ and $\varphi \to \pi/2$ as $H \to +0$. By formal reversal of the sign of H (equivalent to the substitution $\beta \to \beta$

$+\pi$) we obtain solution with $\varphi \to \pi+\beta$ as $H \to -\infty$ and $\varphi \to 3\pi/2$ as $H \to -0$. Thus, on passing through the point $H=0$ the angle φ jumps from $\pi/2$ to $3\pi/2$, i.e., the signs of the vectors l and m are reversed.

4. MEASUREMENT SETUP AND PROCEDURE

A diagram of the setup for the investigation of birefringence in a magnetic field upon application of mechanical stresses is shown in Fig. 2. The source of the $\lambda = 1.15$ μm radiation was helium-neon laser *1*. The polarizer *4* and analyzer *14* were Glan-Thompson prisms. The quarter-wave plate *3* was used to produce circularly polarized light, and quarter-wave plate *11* served to analyze the radiation passing through the crystal. The radiation was modulated with a rotating Glan-Thompson prism *12* mounted on the hollow shaft of synchronous motor *13*. The motor is energized from generator *19* through power amplifier *20*. The signal from photoreceiver *15* passed through a twin-*T* bridge *16* to narrow-band amplifier *17* and next to synchronous detector 18, to which a reference voltage was applied from a sound generator. The synchronous-detector output signal could be registered with *x-y* recorder *21* as a function of the magnetic field H_x in the gap of electromagnet *5*. The vertical coils *6* were used either to produce the constant vertical component of the magnetic field, or for constant displacement of the magnetic field from a position strictly perpendicular to p, with successive switching to the windings of the electromagnet.

The hematite samples, plates of thickness $d=0.3$ mm, were glued into a holder that made it possible to apply a tensile stress up to 150 kgf/cm^2. Figure 2 shows in detail the holder construction. In the course of the experiment it was possible to illuminate the central part of the sample and to vary the illuminated region from 1 to 0.1 mm. The U_2 axis of the samples was oriented perpendicular to p accurate to ±3°.

As already noted, the measurements are based on modulation of the light flux with a rotating polarizer.

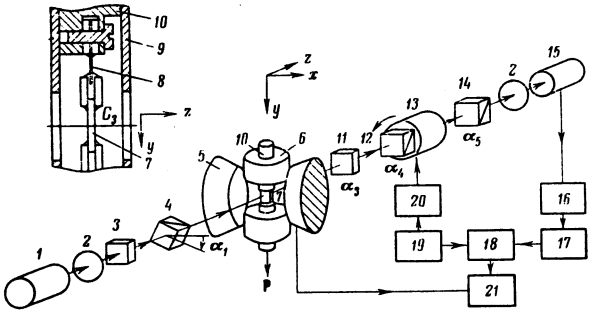

FIG. 2. Experimental setup for magneto-optical investigations: *1*—laser, *2*—lens, *3*, *11*—quarter-wave plates; *4*, *14*—Glan-Thompson prisms, *5*—electromagnet, —vertical coils, *7*—sample, *8*—elastic film, —guiding tube, —immobile piston, *12*—rotating Glan-Thompson prism, *13*—synchronous motor of modulator, *15*—photodetector, 16—twin-*T* bridge, *17*—narrow-band amplifier, *18*—synchronous detector, *19*—sound generator, *20*—power amplifier, *21*—*x-y* recorder.

This method permits direct measurement of the components of the dielectric tensor. Let us examine this method in greater detail. The intensity of the radiation that passes through an optical system made up of arbitrarily oriented polarizers and birefringent medium, such as shown in Fig. 2, is given by the following formula, which is derived by Muller's method[11]:

$$I = {}^1/_4 I_0 (1+C_{51})(1+C_{43}C_{32}C_{21} - C_{43}S_{32}S_{21}\cos\varkappa - S_{43}S_{32}C_{21}\cos\theta + S_{43}S_{21}\sin\theta\sin\varkappa - S_{43}C_{32}S_{21}\cos\theta\cos\varkappa), \quad (14)$$

where I_0 is the radiation intensity past the first polarizer,

$$S_{ij} = \sin 2(\alpha_i - \alpha_j), \quad C_{ij} = \cos 2(\alpha_i - \alpha_j); \quad i, j = 1, \ldots, 5,$$

$\alpha_1, \alpha_2 \equiv \alpha, \alpha_3, \alpha_4, \alpha_5$ are the azimuths of the polarizer transmission axes and the highest-velocity of the birefringent media, respectively, $\varkappa$ is the phase shift corresponding to the crystal *7*, and $\theta = \pi/2$ is the phase shift of the quarter-wave plate *11*.

Let now $\alpha_1 = 0$, $\alpha_2 = \alpha$, $\alpha_3 = 0$, $\alpha_4 = \Omega t$, and α_5 arbitrary; Eq. (14) yields then the intensity of the second harmonic:

$$I(2\Omega) = {}^1/_4 I_0 [(\sin\varkappa\sin 2\alpha + \sin 2\alpha_5)\sin 2\Omega t + (1-\cos\varkappa)\sin^2 2\alpha\cos 2\Omega t]. \quad (15)$$

If a signal proportional to $I(2\Omega)$ is applied to the synchronous detector, which receives in turn a reference signal $U_0 \sin 2\Omega t$, then the output voltage is

$$U_1 = k(\sin\varkappa\sin 2\alpha + \sin 2\alpha_5), \quad (16)$$

since the voltage at the output detector is $U_{out} \sim U_{in}\cos\delta$, where is the phase shift between the input and reference voltage, and U_{in} is the amplitude of the input signal.

In the case of small phase shifts we can put $\sin\varkappa \approx \varkappa$ ($\varkappa < 30°$ in the experiment) and then, using the rotation

$$\varkappa\sin 2\alpha = 2\pi d\varepsilon_{xy}/\lambda n_0, \quad (17)$$

we get

$$U_1 = k(2\pi d\varepsilon_{xy}/\lambda n_0 + \sin 2\alpha_5). \quad (18)$$

Similarly, if

$$\alpha_1 = \pi/4, \ \alpha_2 = \alpha, \ \alpha_3 = \pi/4, \ \alpha_4 = \Omega t$$

and the reference signal is $U_0 \cos 2\Omega t$, then the output of the synchronous detector is

$$U_2 = k\left(\frac{2\pi d}{\lambda n_0}\frac{\varepsilon_{xx}-\varepsilon_{yy}}{2} + \cos 2\alpha_5\right). \quad (19)$$

On the basis of (18) and (19) we can propose two methods for determining the components of the dielectric tensor. In the first we determine the analyzer position α_5 for which the synchronous detector signal is zero. In this case

$$\sin 2\alpha_5|_{U_1=0} = -\frac{2\pi d}{\lambda n_0}\varepsilon_{xy}, \quad \cos 2\alpha_5|_{U_2=0} = -\frac{2\pi d}{\lambda n_0}\frac{\varepsilon_{xx}-\varepsilon_{yy}}{2}.$$

In the second method one measures the signals U_1 and U_2 at fixed values of α_5 (it is convenient to use $\alpha_5 = \pi/2$ and $\alpha_5 = -\pi/4$ when measuring U_1 and U_2, respectively).

An advantage of the first method is that it yields absolute values that are independent of the radiation intensity and of the gain of the entire system, with the accuracy determined principally by the accuracy of the

analyzer dial. An advantage of the second method is the possiblity of automatically recording small changes of the dielectric-tensor components. The analyzer is needed here only to determine the null level and to calibrate the entire channel.

We note that the traditional method of determining the values of α and $\varkappa$ by simultaneously rotating the polarizer, the analyzer, and the quarter-wave plate is quite cumbersome, let alone the complexity of automation of the measurements.

It must be noted that formulas (18) and (19) were derived for a homogeneous medium. We have investigated here samples in which domains could be formed. The components ε_{ij} in (18) and (19) are in this case quantities averaged over all the domains in the illuminated part of the sample. If the domain dimensions greatly exceed the radiation wavelength and the phase shifts are small, the following formula holds:

$$\varepsilon_{ij}=\frac{1}{V}\sum_{k}V_k\varepsilon_{ij}^{(k)}, \qquad (20)$$

where V_k is the volume of a domain having a dielectric tensor $\varepsilon_{ij}^{(k)}$; the summation is over all domains in the illuminated volume of the sample V.

5. DISCUSSION OF EXPERIMENTAL RESULTS

In the absence of mechanical stresses, in a magnetic field $H>2$ kOe parallel to the x axis, the quantity $\frac{1}{2}(\varepsilon_{xx}-\varepsilon_{yy})$ for hematite is constant and is the sum of the magnetic and magnetostriction contributions to the birefringence, equal to $\eta+\eta'=5.8\times10^{-4}$. Application of mechanical tensile stresses p decreases $\frac{1}{2}(\varepsilon_{xx}-\varepsilon_{yy})$ in accord with Eq. (5). The proportionality coefficient yields the piezo-optical constant

$$\zeta=^1/_2\partial(\varepsilon_{xx}-\varepsilon_{yy})/\partial p=-0.8\cdot10^{-6}\ \text{cm}^2/\text{kgf}.$$

Application of a stress $p_s=13$ kgf/cm^2 cancels the magnetostriction contribution, whose value turned out to be $\eta'=-\zeta p_s\approx10^{-5}$. It can therefore be concluded that the ratio of the magnetostriction contribution to the pure magnetic contribution amounts to $\eta'/\eta\approx0.02$. Consequently, the birefringence in hematite is due mainly to the magnetic subsystem.[4)]

Figure 3 shows plots of the dielectric-tensor components $\frac{1}{2}(\varepsilon_{xx}-\varepsilon_{yy})$ and ε_{xy} against the magnetic field at various tensile stresses. The angle of disorientation of p and H from mutual perpendicularity was[5)] $\beta=3°$.

At a stress 4.2 kgf/cm^2 minimal load, corresponding to the weight of the moving piston), the value of $\frac{1}{2}(\varepsilon_{xx}-\varepsilon_{yy})$ increases sharply with increasing magnetic field, and remains unchanged at $H>1$ kOe, corresponding to the transition of hematite from a multidomain state into a single domain relative to the vector m. At stresses exceeding 100 kgf/cm^2, the rotation of the vector l from the position $\mathbf{l}\perp\mathbf{H}$ to the position $\mathbf{l}\perp\mathbf{p}$ proceeds in almost single-domain fashion. From these data and Eqs. (5) we obtained the values of the angle φ as a function of H, as shown in Fig. 4. The solid line is a theoretical curve calculated for $\beta=3°$ and $m_C/2(U_{12}-U_{11})=1.45\times10^5$

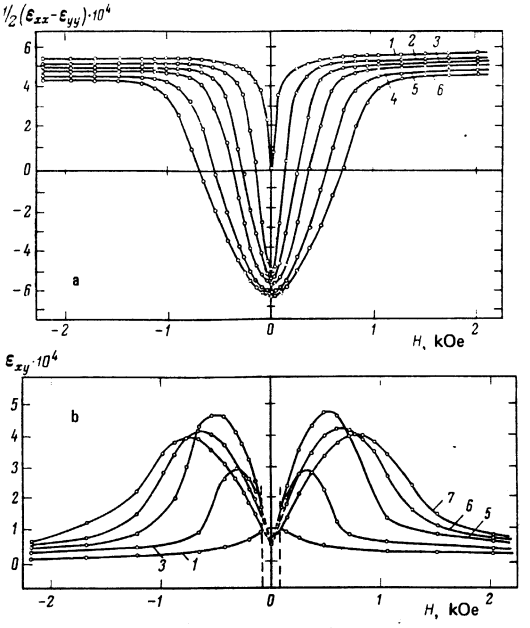

FIG. 3. Plots of the components $1/2(\varepsilon_{xx}-\varepsilon_{yy})$ (a) and ε_{xy} (b) against H at $\beta=3°$, and at tensile stresses: 1) 4.2, 2) 34, 3) 55.4, 4) 83, 5) 11, 6) 136, and 7) 150 kgf/cm^2.

Oe by formula (10, neglecting the last term, a procedure permissible in weak magnetic fields $H\ll20$ kOe. It is seen from Fig. 4 that at all mechanical stresses the vector l rotates in the same manner as a function of the magnetic field, and all that changes is the scale of variation of the magnetic field.

In the vicinity of $H=0$, the $\varepsilon_{xy}(H)$ curves (Fig. 3b) reveal hysteresis (the hysteresis region is bounded by dashed lines). Figure 5 shows a plot of typical hysteresis at $p=122$ kgf/cm^2 and $\beta=3°$. The presence of hysteresis and of jumps on this curves is evidence of a phase transition between two single-domain states, l, $\mathbf{m}\to-\mathbf{l}$, m at $H=0$, in agreement with the theoretical analysis. The width of the hysteresis in Fig. 5 amounted to ~40 Oe and remained essentially unchanged when the recording rate was changed from several seconds to several minutes. It appears that this transition takes place in the usual manner, via motion of the domain walls that separate one phase from the always-present germs of another phase.

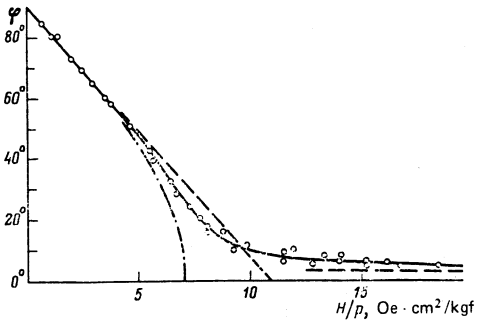

FIG. 4. Plot of the angle φ against H/p at $\beta=3°$. Solid line—theoretical curve (100 kgf/cm^2 $<p<$ 150 kgf/cm^2), dash-dot—theoretical curve for $\beta=0$.

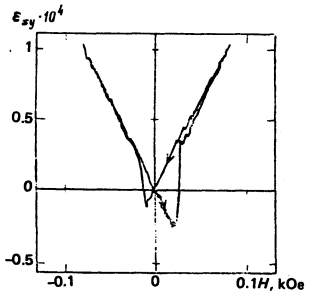

FIG. 5. Plot of the component ε_{xy} in weak fields at $\beta = 3°$ and $p = 122$ kgf/cm^2.

If p is strictly perpendicular to H($\beta = 0$), jumps and hysteresis are observed on the $\varepsilon_{xy}(H)$ curves. The values of the jumps and the hysteresis behavior changed significantly when the dimensions and location of the illuminated region of the sample were changed. Figure 6 shows a plot of $\varepsilon_{xy}(H)$ at $\beta = 0$, $p = 122$ kgf/cm^2, and an illuminated-region diameter of approximately 1 mm.

The jumps and the hysteresis demonstrate that the sample breaks up into domains with different values of φ. The plot of $\varepsilon_{xy}(H)$ at an illumination region of about 0.1 mm, shown in Fig. 7, indicates that the breakup into domains with different φ exists upt to $\beta = 1.5°$. The jumps observed on these curves reached values comparable with the maximum value of $\varepsilon_{xy}(H)$ (curve 1), thus indicating that the characteristic domain dimension in the basal plane is about 0.1 mm.

The plots of $\frac{1}{2}(\varepsilon_{xx} - \varepsilon_{yy})$ against H are not sensitive to domain formation and reveal no jumps typical of the $\varepsilon_{xy}(H)$ plots. At $\beta \sim 0°$ they are of the same form as in Fig. 3a, but the transition becomes steeper near $H_{cr}(p)$. Nevertheless, the kink at $H = H_{cr}(p)$ predicted by the simplest theory is not observed on these curves at $\beta = 0°$.

The value of $\frac{1}{2}(\varepsilon_{xx} - \varepsilon_{yy})$ can be insensitive to domain formation if

$$\tfrac{1}{2}(\varepsilon_{xx} - \varepsilon_{yy}) = (\eta + \eta')\cos 2\varphi + \zeta p$$

has the same value for different domains, and this is possible only if the values of φ for the different domains differ in sign only. This confirms, in turn, the theoretical conclusion that the transition is even in φ.

The question of the behavior of hematite when a force

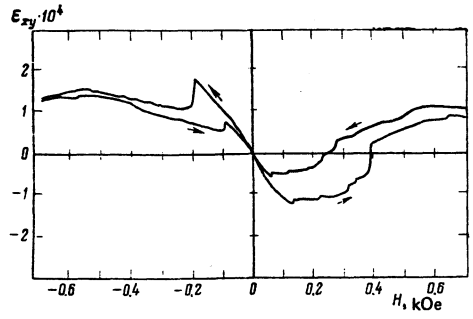

FIG. 6. Plot of ε_{xy} against H at $\beta = 0°$, $p = 122$ kgf/cm^2, diameter of illuminated region of sample 1 mm.

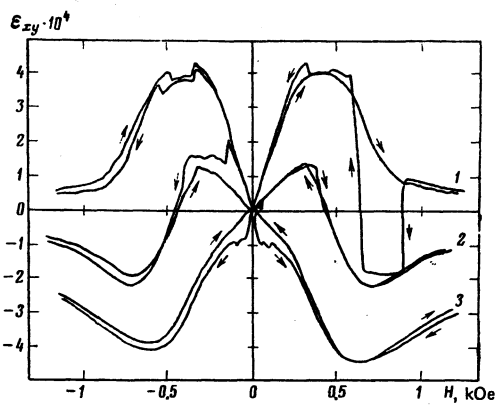

FIG. 7. Plots of ε_{xy} against H at $p = 122$ kgf/cm^2 and diameter of illuminated region of sample 0.1 mm; curves: 1) $\beta = +1.5°$, 2) $\beta = 0°$, 3) $\beta = -1.5°$.

is applied in the basal plane was raised in connection with the investigation of antiferromagnetic resonance (AFMR).[15,16] Investigations by a number of workers have led to the following hypothesis that reflect individual aspects of the behavior of hematite and manifest themselves indirectly in the experimental results on AFMR:

1) When an external force is applied in a direction such as to cancel the magnetostriction, the magnetic subsystem does not change its equilibrium position in a sufficiently strong field.[15]

2) When the sample is compressed along $H \to 0$ at $p \geq p_c$, the vector l is oriented along $H \to 0$ (sublattice flipping induced by directed compression), and an increase of H deflects the vector l away from the position

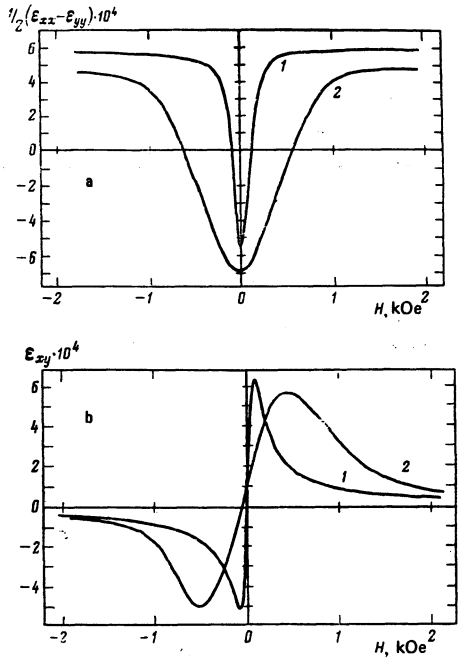

FIG. 8. Plots of the components $1/2(\varepsilon_{xx} - \varepsilon_{yy})$ (a) and ε_{xy} (b) against H following application of a constant vertical magnetic field $h = 70$ Oe and at $p = 4.2$ kgf/cm^2 (1) and $p = 122$ kgf/cm^2 (2).

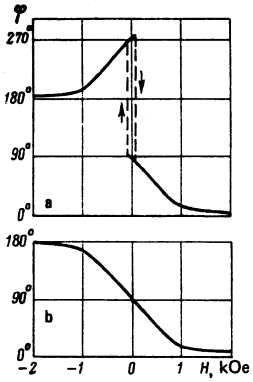

FIG. 9. Plots of rotation angle of antiferromagnetic vector in the multidomain state at $p = 122$ kgf/cm^2 and $\beta = 3°$ (a), $h = 70$ Oe (b).

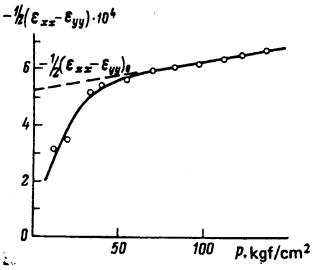

FIG. 10. Plot of $1/2$ $(\varepsilon_{xx} - \varepsilon_{yy})$ against p at $H = 0$.

at $H \to 0$; jumplike changes of the orientation of **l** are not excluded.[16]

3) When mechanical stresses are produced, there exists a certain critical magnetic field such that at $H \geq H_{cr}$ the magnetic subsystem does not change orientation (it corresponds to item 1) above), and when $H \leq H_{cr}$ the vector **l** moves continuously ways from the position $\mathbf{l} \perp \mathbf{H}(H = H_{cr})$ into the position $\mathbf{l} \parallel \mathbf{H}(H \to 0)$.[10]

It follows from described direct measurement of the orientation of the vector **l** that there exist values of **p** and **H** such that the vectors **m** and **l** do not change their positions, and values of **p** and **H** such that **m** and **l** become smoothly reoriented. The character of the transition is strongly influenced by the mutual orientation of the vectors **p** and **H**. If **H** is strictly perpendicular to **p**, the sample always breaks up into domains that have different signs of φ.

Formation of domains can be prevented either by deflecting **H** away from the position $\mathbf{H} \perp \mathbf{p}$, or by applying a constant magnetic field $\mathbf{h} \parallel \mathbf{p}$. Plots of ε_{xy} and $\frac{1}{2}(\varepsilon_{xx} - \varepsilon_{yy})$ at $h = 70$ Oe are shown in Fig. 8 ($p = 122$ kgf/cm^2). We note that in this case $\varepsilon_{xy}(H)$ changes substantially in this case, namely, it becomes odd.

The experimental data were used to determine the angle φ. For comparison, Fig. 9 shows plots of φ at weak disorientation $\beta = 3°$ and when a weak vertical field is applied. It is important that without application of $\mathbf{h} \parallel \mathbf{p}$ the direction of the vector **l** at $H = 0$ is almost completely reversed (Fig. 9a); this is reflected in the jumps of the angle φ from 90° to 270°. When a field $h = 70$ Oe is applied, this jump vanishes and the rotation in the entire range of fields is that of a single domain (Fig. 9b).

In conclusion, let us dwell on the variation of the birefringence in hematite when mechanical stress is applied in the absence of a magnetic field, as shown in Fig. 10. When the voltage changes from 0 to ~50 kgf/cm^2, hematite changes from the multi-domain state brought about by the natural third-order anisotropy in the basal plane into a state with $\mathbf{l} \perp \mathbf{p}$, which is also multidomain, with the domains differing in the signs of **l** and **m**. The birefringence in the type of domain is the same. The bend of the plot of $\frac{1}{2}(\varepsilon_{xx} - \varepsilon_{yy})$ at $p \gtrsim 50$ kgf/cm^2 is due to the photoelastic effect, and the *dc* component $-\frac{1}{2}(\varepsilon_{xx} - \varepsilon_{yy})$ at $p \to 0$ is of magnetic origin (accurate to 2%).

Thus, by using a specially developed procedure to determine small changes of the dielectric-tensor components of a birefringent medium, we have demonstrated experimentally that the main contribution to birefringence in hematite, when radiation propagates along the C_2 axis, is purely magnetic, while the magnetostriction effect is about two per cent of the total effect. We have observed directly and monitored with high accuracy the reorientation of the antiferromagnetism vector in the basal plane in magnetic anf force fields at $T = 300$ K. Antiferromagnetic domains in the region of the orientational transition were observed and investigated; methods of making the sample single-domain by displacing the magnetic field from the position $\mathbf{H} \perp \mathbf{p}$ and by applying a constant magnetic field $\mathbf{h} \parallel \mathbf{p}$ were proposed. It was observed that at a pressure $p \gtrsim 50$ kgf/cm^2, in the absence of a magnetic field, a transition takes place from the multidomain state due to the natural third-order anisotropy into a single-domain strate with oppositely directed **l** and **m** in the different domains.

In conclusion, the authors thank Academician A. M. Prokhorov and the scientific director of SNRS (France), Dr. J. Winter, for support and for a discussion of the joint work.

[1)] SNRS Laboratory of Magnetism and Optics of the Solid State, Bellevue, France.

[2)] Measured in the present study.

[3)] In this paper we do not discuss one of the possible contributions made to magnetic birefringence by an asymmetrical displacement of the equilibrium position of the atoms without change in the volume of the unit cell, corresponding to a "frozen-in" optical phonon with wave vector $k = 0$. [6]

[4)] It should be noted that the question of the ratio of the various contributions to birefringence in magnetically ordered crystal was investigated in studies of iron-garnet systems. [12-14] It was concluded that the magnetostriction contribution is small. However, the interpretation of results obtained for such complicated systems as garnet is not simple.

[5)] Figures 3 and 7 show the values of the dielectric-tensor components in terms of a laboratory coordinate system in which the x axis is directed along the magnetic field. In the remaining figures the orientation is the same as in Fig. 1.

[1] A. N. Winchell and H. Winchell, Microscopical Characters of Artificial Inorganic Solid Substances; Optical Properties of Artificial Minerals; Academic, 1964.

[2] R. V. Pisarev, I. G. Siniĭ, and G. A. Smolenskiĭ, Pis'ma Zh. Eksp. Teor. Fiz. **9**, 112 (1969) [JETP Lett. **9**, 64 (1969)].

[3]H. M. A. Urquhart and J. E. Goldman, Phys. Rev. **101**, 1443 (1956).
[4]V. S. Merkulov and E. G. Rudashevskiĭ, All-Union Conf. on the Physics of Magnetic Phenomena, Abstracts "ELM," Baku, 1975, p. 67.
[5]V. S. Merkulov, E. G. Rudashevskiĭ, and H. Le Gall, Pis'ma Zh. Eksp. Teor. Fiz. **22**, 140 (1975) [JETP Lett. **22**, 64 (1975)].
[6]W. Jauch and H. Dachs, Solid State Commun. **14**, 657 (1974).
[7]R. Z. Levitin, A. S. Pakhomov, and V. A. Shchurov, Zh. Eksp. Teor. Fiz. **56**, 1242 (1969) [Sov. Phys. JETP **29**, 669 (1969)].
[8]J. F. Reintjes and M. B. Schulz, J. Appl. Phys. **39**, 5254 (1968).
[9]I. E. Dzyaloshinskiĭ, Zh. Eksp. Teor. Fiz. **33**, 1454 (1958) [Sov. Phys. JETP **6**, 1120 (1958)].
[10]I. E. Dikshteĭn, V. V. Tarasenko, and V. G. Shavrov, Fiz. Tverd. Tela (Leningrad) **16**, 2192 (1974) [Sov. Phys. Solid State **16**, 1432 (1975)].
[11]W. A. Shurcliff, Polarized Light, Harvard, 1962.
[12]L. M. Dedukh and V. I. Nikitenko, Fiz. Tverd. Tela (Leningrad) **12**, 1768 (1970) [Sov. Phys. Solid State **12**, 1400 (1970)].
[13]R. T. Lynch, J. F. Dillon, and L. G. Van Uitert, J. Appl. Phys. **44**, 225 (1973).
[14]R. V. Pisarev, N. N. Kolpakova, A. G. Titova, and L. M. Dashevskaya, Fiz. Tverd. Tela (Leningrad) **17**, 56 (1975) [Sov. Phys. Solid State **17**, 31 (1975)].
[15]A. S. Borovik-Romanov and E. G. Rudashevskiĭ, Zh. Eksp. Teor. Phys. **47**, 2095 (1965) [Sov. Phys. JETP **20**, 1407 (1965)].
[16]P. P. Maksimenkov and V. I. Ozhogin, Zh. Eksp. Teor. Fiz. **65**, 657 (1973) [Sov. Phys. JETP **38**, 324 (1974)].

Translated by J. G. Adashko

Photogalvanic effect due to free carriers in noncentrosymmetric crystals

V. I. Belinicher

Institute of Automation and Electrometry, Siberian Branch of the Academy of Sciences of the USSR, Novosibirsk
(Submitted 21 February 1978)
Zh. Eksp. Teor. Fiz. **75**, 641–652 (August 1978)

An analysis is made of the photogalvanic effect in semiconductors and metals in the case when the frequency of light is insufficient for impurity–band and band–band transitions. It is shown that the photocurrent appears because of the asymmetry of the scattering of electrons (holes) by impurities, phonons, and electrons (holes) in the field of a light wave, and that the magnitude of this photocurrent is proprotional to the coefficient of absorption of light. The order of magnitude of the photocurrent normalized to the absorption coefficient is the same as that for band–band optical transitions.

PACS numbers: 72.40.+w, 72.20.Dp, 63.20.Kr, 71.38.+i

1. INTRODUCTION

The photogalvanic effect is the appearance of a static photocurrent in a homogeneous noncentrosymmetric crystal under the action of homogeneous illumination: it has been observed in several experiments.[1-3] The microscopic theory of the effect is proposed in Refs. 4–6. However, this theory is limited to the case of impurity–band[5] and band–band[6] optical transitions.

The microscopic mechanism of the photogalvanic effect in noncentrosymmetric semiconductors is discussed by Genkin and Mednis[7,8] in the case when the photon energy is insufficient for band–band optical transitions. Genkin and Mednis allow for virtual optical transitions of an electron to other bands of a semiconductor, which results in the asymmetry of the renormalization of the electron dispersion law in the case of elliptically polarized light. However, this asymmetry does not give rise to a static photocurrent. The photocurrent J can be found by integration with respect to the quasimomentum k:

$$\mathbf{j}=\int \nabla_{\mathbf{k}}\varepsilon_{\mathbf{k}} f_{\mathbf{k}}\, d\mathbf{k}. \qquad (1)$$

Illumination alters both the dispersion law of electrons $\varepsilon_{\mathbf{k}}$ and their distribution function $f_{\mathbf{k}}$. The change in the function $f_{\mathbf{k}}$ due to illumination is ignored by Genkin and Mednis.[7,8] This change is due to intraband electron scattering processes. In the principal approximation, we find that $f_{\mathbf{k}}$ remains the Boltzmann distribution function even if allowance is made for scattering but this distribution function is now coupled to an asymmetric dispersion law. In this approximation, the photocurrent (1) vanishes since the total derivative in respect of the quasimomentum k occurs in the integral (1). The formal mechanism responsible for the vanishing of the photocurrent[7,8] is discussed in the present paper.

We shall be concerned with the photogalvanic effect due to free carriers in noncentrosymmetric semiconductors and metals.

We shall obtain an exact expression for the tensor of the photogalvanic effect (photogalvanic tensor) β_{iln} using the Keldysh diagram technique[9] (analog of the Kubo formula) and consider various mechanisms of electron scattering by impurities and phonons and the electron–electron scattering in metals in the presence of a light wave. The scattering asymmetry[5] in noncentrosymmetric crystals is responsible for the appearance of a

 0038-5646/78/080322-06$02.40